Modelling non-steady flight regimes of a hingeless rotor helicopter.

A.O. Garipov, A.M. Girfanov, S.A. Mikhailov, and E.I. Nikolaev

A.N. Tupolev Kazan State Technical University, Kazan Helicopters JSC
Kazan, Russia

Abstract

The goal of this paper is to consider problems of mathematical modelling of non-steady flight regimes of a helicopter equipped with a main rotor hingeless hub, as well as helicopter controlled motion. The technique suggested is based on numerical integration with respect to time using expansion of blade strains, and the calculation results by this technique are presented. The design loads are compared with the experimental ones. The paper also describes the results of modelling dynamics of a helicopter with a main rotor hingeless hub in flight by autopilot to improve stability and controllability.

Introduction

At the present-day stage, the helicopter development follows the way of improving the consumer properties, lower service cost, reduced noise level, improved stability and controllability, higher manoeuvrability. One of the main lines in the rotorcraft development is the improvement of their lifting system followed by a wide use of modern composite materials. Therefore, most present-day helicopters have main rotors with "hingeless hubs" and the function of hinges is performed by special elastic elements. Such rotors possess a number of advantages over conventional rotors equipped with flapping, feathering and lag hinges:

- design simplicity;
- low cost and simple maintenance (no lubrication points);
- increased structure lifetime;
- large controlling moments at the hub and others.

Another promising line in the helicopter improvement is the use of digital (analogue) systems of electric remote control integrated with automatic control systems. These systems make it possible to significantly improve helicopter stability and controllability, increase its manoeuvring characteristics and reduce the structure weight.

Although large controlling moments at the hub increase helicopter manoeuvring characteristics, at the same time they reduce its lifetime and increase loads on the main rotor shaft. To predict the load level, the structure operation must be analysed not only at the steady-state (cruising) regimes, but also during manoeuvres.

This paper deals with the problems of mathematical modelling of non-steady flight regimes of a helicopter equipped with a main rotor hingeless hub. As calculation cases the following regimes are presented: helicopter acceleration, climbing, descent and flight with vertical over loads. The results of flight tests of a light multipurpose helicopter "Ansat" designed at Kazan Helicopters JSC were used to adjust a mathematical model and compare the results obtained with the experimental data. This helicopter is equipped with a main rotor hingeless hub and a digital electric remote control systems which includes a system for improving stability and controllability and an automatic control system. All these systems are combined into a helicopter integrated control system (ICS).

Fig. 1 Light multipurpose helicopter "Ansat".

The proposed paper also presents the results of mathematical modelling of the "Ansat" helicopter flight dynamics in ICS operation exemplified by stability of helicopter lateral motion.

Mathematical model of a hingeless main rotor

An important component of the mathematical model proposed is a technique of numerical integration with respect to time using the blade strain expansion into the Fourier trigonometric series. A peculiarity of this technique is a fortiori known dependence between deflections, velocities and accelerations of design blade points. This dependence makes it possible to basically change a way of searching for a solution by azimuth and get rid of iterations connected with the determination of velocity and acceleration. Such an approach significantly reduces time necessary to obtain the rotor aeroelastic characteristics and, hence, the loads on the helicopter lifting system on the whole, while the calculation accuracy is retained.

Determination of a blade elastic line

Taking into account the model accepted, the position of a blade elastic line is specified with the

aid of angular functions $\xi(r,\psi)$, $\eta(r,\psi)$, $\zeta(r,\psi)$ [1]. At the quasi-steady regimes they are the periodic functions and can be expanded into the Fourier series in terms of azimuth (time).

$$\xi_n = a_{0n}^{\xi} + \sum_{k=1}^{\infty}\left(a_{kn}^{\xi}\cdot\cos k\psi + b_{kn}^{\xi}\cdot\sin k\psi\right);$$

$$\eta_n = a_{0n}^{\eta} + \sum_{k=1}^{\infty}\left(a_{kn}^{\eta}\cdot\cos k\psi + b_{kn}^{\eta}\cdot\sin k\psi\right); \quad (1)$$

$$\zeta_n = a_{0n}^{\zeta} + \sum_{k=1}^{\infty}\left(a_{kn}^{\zeta}\cdot\cos k\psi + b_{kn}^{\zeta}\cdot\sin k\psi\right),$$

where a_0^{ξ}, a_k^{ξ}, b_k^{ξ}, a_0^{η}, a_k^{η}, b_k^{η}, a_0^{ζ}, a_k^{ζ}, b_k^{ζ} are the expansion coefficients; $\psi = \omega\cdot t$ is the blade azimuth; k – is the number of expansion harmonics.

If the values of the expansion coefficients are known, the deflections, as well as velocities and accelerations of any blade point can be calculated in the coordinate system chosen:

$$x_n = \int_{s_0}^{s_n}\sin\eta ds + C_1;$$

$$y_n = -\int_{s_0}^{s_n}\sin\xi\cos\eta ds + C_2; \quad (2)$$

$$z_n = \int_{s_0}^{s_n}\cos\xi\cos\eta ds + C_3;$$

$$\dot{x}_n = \int_{s_0}^{s_n}\dot{\eta}\cos\eta ds + C_4;$$

$$\dot{y}_n = -\int_{s_0}^{s_n}\dot{\xi}\cos\xi ds + C_5; \quad (3)$$

$$\dot{z}_n = \int_{s_0}^{s_n}\left(\dot{\xi}\sin\xi - \dot{\eta}\sin\eta\right)ds + C_6;$$

$$\ddot{x}_n = \int_{s_0}^{s_n}\ddot{\eta}\cos\eta ds + C_7;$$

$$\ddot{y}_n = -\int_{s_0}^{s_n}\ddot{\xi}\cos\xi ds + C_8; \quad (4)$$

$$\ddot{z}_n = \int_{s_0}^{s_n}\left(\ddot{\xi}\sin\xi - \ddot{\eta}\sin\eta\right)ds + C_9$$

The integration constants $C_1 - C_9$ are determined by the conditions of blade attachment to the rotor hub.

The above relations allow all parameters of the blade spatial motion to be found at the well-known expansion coefficients. Thus, the expansion coefficients sought to be determined for solving a system of equations are taken as basic unknowns. Any periodic function can be described if the number of harmonics is $k \to \infty$. However, the finite number of expansion harmonics K is necessary for practical application. Then, $M = 3\cdot(2\cdot K+1)$ unknowns will be on one radius by azimuth. Taking into account the number of points along the blade radius N, the number of unknowns will be $P = M\cdot N$.

To calculate P parameters, the same number of equations is needed. There are three equations in each blade node at the azimuth specified, and the required number of equation can be obtained if the pitch by azimuth is $\Delta\psi = \frac{2\pi}{2K+1}$. The final system of nonlinear integral equations will consist of $M\cdot N$ equations of blade spatial vibrations.

Thus, the solution of the blade vibrations equation is reduced to finding the coefficients of blade displacement expansion into the Fourier series in terms of azimuth with a specified accuracy. The solution of a system of equilibrium equations results in the rotor characteristics per a blade revolution.

Determination of main rotor induced velocities

The formulas based on the results of the classic vortex theory for a main rotor proposed in [2] are used to calculate the non-uniform distribution of induced velocities.

The average value of induced velocities along the main rotor disk is calculated by the formula:

$$V_0^i = \frac{1.2}{\sqrt{\mu^2+\lambda^2}}\left[\frac{C_T}{4} - \frac{\mu\cdot tg^2\lambda\cdot 1.38}{4\left(1+32\cdot\lambda^2/C_T\right)\left(1+32\cdot\mu^2/C_T\right)}\right], \quad (5)$$

were $\mu = \frac{V\cos\alpha}{\Omega R}$ is the characteristic of the rotor operating regime; $\lambda = \frac{V\sin\alpha + V_0^i}{\Omega R}$ is the disk flow ratio.

For the specified C_T, the induced velocities V_0^i are calculated by the successive approximation method. If $V_0^i = \frac{C_T}{2\sqrt{\mu^2 + C_T/2}}$ is taken as a first approximation, the process converges for three or four iterations.

The linear distribution of the disk flow velocities is used in the value V_0^i as a first approximation to the real nonuniform distribution:

$$W_0^i = V_0^i \begin{bmatrix} f_1 \cdot \sqrt{r \cdot 1.5} + \\ f_2 \left(1 + k_x \cdot r \cdot \cos\psi + k_y \cdot r \cdot \sin\psi\right) \end{bmatrix}; \quad (6)$$

were

$f_1 = 1 - f_2$;

$f_2 = 13.5 \cdot \mu$, but $f_2 \le 1.0$;

$k_x = \frac{4}{3}\left[\left(1 - 1.8 \cdot \mu^2\right)\sqrt{1 + \left(\lambda/\mu\right)^2} - \lambda/\mu\right]$;

$k_y = -2\mu$.

Thus, at the relative velocities $\mu < 0.074$ the funnel-shaped distribution of induced velocities can smoothly change to a distribution in the form of a skewed cylinder at high velocities.

Determination of aerodynamic loads acting on a blade

The aerodynamic load on the main rotor blades is calculated on the basis of the blade element theory. This theory is based on the assumption that each element of the rotor blade can be considered as a profile section moving in a helix. The lift and drag are calculated from the resulting velocity of the incoming flow. It is considered that the blade parts adjacent to the section under consideration have no influence on its aerodynamic characteristics. The rotor shaft thrust and torque are calculated by integration of elementary forces and moments of individual blade elements with respect to the radius.

To obtain reliable results in the calculations of aerodynamic loads with the use of model wind tunnel tests, the profile aerodynamic characteristics were recalculated by the Reynolds similarity criterion and the Mach number for each design blade section.

Determination of inertial loads acting on a blade

The position of the *i*-th blade point is completely described by the radius-vector:

$$\overline{R}_i = \overline{R}_0 + \overline{r}_i, \quad (7)$$

where $\overline{R}_0$ is the radius-vector of the pole *O* with respect to the stationary coordinates; $\overline{r}_i$ is the radius-vector of the *i*-th blade point in the body-axes.

The expression for determination the mass-inertia forces acting on the *i*-th blade element has the form:

$$\overline{F}_i = m_i\left[\ddot{\overline{r}}_i + \dot{\overline{\Omega}} \times \overline{r}_i + 2\ \overline{\Omega} \times \dot{\overline{r}}_i + \overline{\Omega} \times \left(\overline{\Omega} \times \overline{r}_i\right)\right]; \quad (8)$$

were $\overline{\Omega}$ is the angular velocity vector of the *i*-th blade point rotation with respect to the rotor hub; m_i is the *i*-th blade element mass.

The expression for determining the mass-inertia moments experienced by the *i*-th blade element has the form:

$$[J]\dot{\overline{\Omega}} + [\dot{J}]\overline{\Omega} + \overline{\Omega} \times [J]\overline{\Omega} + \overline{r}_i \times m_i \ddot{\overline{r}}_i + \overline{\Omega} \times \left(\overline{r}_i \times m_i \dot{\overline{r}}_i\right) = \overline{r}_i \times \overline{F}_i \quad ; \quad (9)$$

where $[J]$ is the inertia tensor of the *i*-th blade element

$$[J] = \begin{bmatrix} J_x & -J_{xy} & -J_{xz} \\ -J_{yx} & J_y & -J_{yz} \\ -J_{zx} & -J_{zy} & J_z \end{bmatrix}. \quad (10)$$

General equation of external forces

In the design section n ($n = 1 \div N$) the external force is known which is presented as the vector of forces per unit length $\overline{t}_n = \{t_{xn}, t_{yn}, t_{zn}\}$ and the vector of bending moments and a torque per unit length $\overline{q}_n = \{q_{xn}, q_{yn}, q_{zn}\}$. Then the equation for the moments of external forces in each design section will be written as follows:

$$M_{xn} = \int_{R_0}^{R} \left[-t_{ym}\left(z_n - z_m\right) + t_{zn}\left(y_n - y_m\right) + q_{xn}\right] dr;$$

$$M_{yn} = \int_{R_0}^{R} \left[t_{xn}\left(z_n - z_m\right) - t_{zn}\left(x_n - x_m\right) + q_{yn}\right] dr; \quad (11)$$

$$M_{zn} = \int_{R_0}^{R} \left[t_{yn}\left(x_n - x_m\right) - t_{xn}\left(y_n - y_m\right) + q_{zn}\right] dr;$$

where x_n, y_n, z_n are the coordinates of the rigidity center line in the blade design sections in the rotating coordinates; x_m, y_m, z_m are the coordinates of the blade attachment point to a torsion bar.

The boundary condition in the blade root will be its attachment to an equivalent hinge with the rigidity concentrated. In this case the difference from a classic hinge is that an elastic moment of resistance to blade rotation is present in this hinge

$$x_0 = 0; \quad y_0 = 0;$$
$$\varphi\left(r_{th}\right) = \varphi_0 - \theta_1 \cdot \sin\psi - \theta_2 \cdot \cos\psi; \quad (12)$$
$$M_\beta\left(r_{fh}\right) = C_\beta \cdot \Delta\beta; \quad M_\eta\left(r_{lh}\right) = C_\eta \cdot \Delta\eta;$$

where C_β, C_η are the rigidity coefficients in the flapping and lag hinges; $\Delta\beta$ and $\Delta\eta$ are the elastic angles of the blade root rotation.

At the free blade end the boundary conditions have the form:

$$Q_x(R) = 0;\ Q_y(R) = 0;$$
$$M_x(R) = 0;\ M_y(R) = 0;\ M_z(R) = 0. \quad (13)$$

They mean that shearing and tensile forces, bending moments and a torque at the free blade end are equal to zero if there are no concentrated loads. The integration constants are calculated from the boundary conditions at the free end and are equal to zero.

Thus, relation (11) makes it possible to determine the blade position depending on external loading.

Loads on the main rotor hub

The concentrated forces that are variable in azimuth and moments with their projections on the rotating coordinates $\overline{P}_r = \{P_{xr}, P_{yr}, P_{zr}\}$, $\overline{M}_r = \{M_{xr}, M_{yr}, M_{zr}\}$ act in the blade root. The average components of forces acting in the non-rotating coordinates of the rotor hub can be calculated as follows:

$$T = \frac{k_b}{2\pi}\int_0^{2\pi} P_{yr} \quad d\psi\ ;$$

$$H = \frac{k_b}{2\pi}\int_0^{2\pi} \left(P_{zr}\cos\psi - P_{xr}\sin\psi\right) d\psi\ ; \qquad (14)$$

$$S = \frac{k_b}{2\pi}\int_0^{2\pi} \left(P_{xr}\cos\psi + P_{zr}\sin\psi\right) d\psi\ ,$$

where k_b is the number of main rotor blades.

Longitudinal and transverse moments experienced by the rotor hub in the non-rotating coordinates are determined as follows:

$$M_{x.mr} = \frac{1}{2\pi}\int_0^{2\pi} (M_{xr}^h \cdot \sin\psi - M_{zr}^h \cdot \cos\psi)\cdot d\psi$$

$$M_{y.mr} = \frac{1}{2\pi}\int_0^{2\pi} M_{yr}^h \cdot \quad d\psi\ ; \qquad (15)$$

$$M_{z.mr} = \frac{1}{2\pi}\int_0^{2\pi} (M_{xr}^h \cdot \cos\psi + M_{zr}^h \cdot \sin\psi)\cdot \quad d\psi\ .$$

Mathematical model of a helicopter

Equations of helicopter motion

A helicopter is considered as an absolutely solid body. The equations describing its motion as a solid body have the form [3]:

$$\begin{cases} m\ \left(\dot{V}_x + \omega_y V_z - \omega_z V_y\right) = R_x - G_x \\ m\ \left(\dot{V}_y + \omega_z V_x - \omega_x V_z\right) = R_y - G_y \\ m\ \left(\dot{V}_z + \omega_x V_y - \omega_y V_x\right) = R_z - G_z \\ J_x\dot{\omega}_x + \left(J_z - J_y\right)\ \omega_z\omega_y = M_x \\ J_y\dot{\omega}_y + \left(J_x - J_z\right)\ \omega_x\omega_z = M_y \\ J_z\dot{\omega}_z + \left(J_y - J_x\right)\ \omega_y\omega_x = M_z \end{cases}; \qquad (16)$$

where $\overline{G}$ is the gravity force applied at the helicopter centre of inertia; $\overline{R}$ and $\overline{M}$ are the main vector and the main moment of aerodynamic and inertia forces; $\overline{\dot{V}}$ is the acceleration of the helicopter centre of inertia; $\overline{\dot{\omega}}$ is the angular acceleration of helicopter rotation relative to its centre of inertia; $\overline{V}$ is the velocity of helicopter centre of inertia; $\overline{\omega}$ is the angular velocity of helicopter rotation relative to the centre of inertia; $\overline{J}$ is the helicopter inertia tensor.

To study the non-steady flight regimes of a helicopter the equations must be supplemented by the equation of main rotor rotation with respect to its axis:

$$J_\omega\ \ \dot{\omega}_{mr} = \xi\ \ M_{en} - M_{mr}\ , \qquad (17)$$

where J_ω is the inertia moment of the main rotor; $\dot{\omega}_{mr}$ is the angular acceleration of the main rotor rotation; M_{en} is the moment supplied to the main rotor shaft from the engine; M_{mr} is the moment of aerodynamic and inertia forces with respect to the main rotor axis; ξ is the engine throttling degree. In more general form the equations of helicopter motion and their derivation are given in [4].

The angles υ, γ and ψ determining orientation of the body-fixed axes in the normal system of coordinates are found as a result of integrating the equations

$$\begin{cases} \dot{\upsilon} = \omega_z\cos\gamma + \omega_y\sin\gamma \\ \dot{\gamma} = \omega_x - \dot{\psi}\sin\upsilon \\ \dot{\psi} = \left(\omega_y\cos\gamma + \omega_z\sin\gamma\right)\big/\cos\upsilon\ . \end{cases} \qquad (18)$$

The motion of the helicopter centre of inertia in the normal ground coordinates is determined from integration of the equations

$$\dot{L} = V_{xg}\ ;\quad \Delta\dot{H} = V_{yg}\ ;\quad \dot{Z} = V_{zg}\ . \qquad (19)$$

Technique for calculating helicopter trim

Trimming is usually divided into longitudinal and lateral trim [5]. This paper deals with an unconventional technique of spatial trim without division into longitudinal and lateral trim [6].

The control required to balance a helicopter is determined from the solution of equation system (16) taking into account equations of connections (18).

The basic unknowns in the system of equations will be presented as column matrix: $\{X\} = \{\varphi_o, \chi, \eta, \varphi_{tr}, \gamma, \vartheta\}^T$ where: φ_0 is the common pitch of the main rotor blades; χ, η are the angles of the cyclic pitch of the main rotor blades; φ_{tr} is the pitch of the tail rotor blades; γ, ϑ are the helicopter rolling and pitching angles, respectively. Then, system of equations (16) can be written in the form: $F(X) = 0$. The solution of the system is reduced to finding of such values of the unknowns X, that satisfy the equation $F(X) = 0$ with the specified accuracy ε. In this paper the Newton method owing to its quadratic convergence is used to search for the solution. This requires that the matrix of partial derivatives be calculated in the form:

$$F' = \begin{bmatrix} \frac{dF_1}{dX_1} & .. & \frac{dF_1}{dX_n} \\ .. & .. & .. \\ \frac{dF_n}{dX_1} & .. & \frac{dF_n}{dX_n} \end{bmatrix} \quad (20)$$

The solution of the balance problem allows its use as the starting point in modelling helicopter flight dynamics.

Modelling helicopter controlled motion

In calculating dynamics not only a helicopter disturbed motion but also motion control must be modelled. At the initial moment of time the position of controls corresponds to the balance values. The displacements of controls during controlled motion can be presented as a sum of increments in the control positions with respect to their position at the initial moment of time. A feedback signal must be added in the presence of automatic stabilization system

$$\begin{aligned} \chi &= \chi_{bal} + \sum_{k=1}^{n} \Delta\chi_{c\,k} + \chi_{fb}; \\ \eta &= \eta_{bal} + \sum_{k=1}^{n} \Delta\eta_{c\,k} + \eta_{fb}; \\ \varphi_0 &= \varphi_{0\,bal} + \sum_{k=1}^{n} \Delta\varphi_{0\,c\,k}; \\ \varphi_{tr} &= \varphi_{tr\,bal} + \sum_{k=1}^{n} \Delta\varphi_{tr\,c\,k} + \varphi_{tr\,fb}. \end{aligned} \quad (21)$$

An increment in the controls positions for each integration step is determined from the expressions:

$$\begin{aligned} \Delta\chi_k &= \dot{\chi}_k \Delta t; \quad \Delta\eta_k = \dot{\eta}_k \Delta t; \\ \Delta\varphi_{0\,k} &= \dot{\varphi}_{0\,k} \Delta t; \quad \Delta\varphi_{tr\,k} = \dot{\varphi}_{tr\,k} \Delta t. \end{aligned} \quad (22)$$

Thus, to determine changes in the controls positions it is sufficient to find an algorithm for varying the velocity of controls reversal in value and direction. The velocity of controls reversal must not exceed a definite maximum value that is permitted by the control system. It is also necessary to take into account limitations on the wobble plate displacement range and variations in the tail rotor common pitch.

In this paper it is suggested that in operation with controls along one channel the pilot stabilizes the helicopter angular position along the remaining channels. It is provided in the model by the following laws of automatic control:

pitch angle stabilization

$$\chi_{fb} = -\left[\left(i_\upsilon^* + k_{\rho\upsilon}\frac{1}{p}\right)\Delta\upsilon + \mu_\upsilon^* \cdot \dot{\upsilon}\right]\frac{1}{\cos\gamma}; \quad (23)$$

roll angle stabilization

$$\eta_{fb} = \left(i_\gamma^* + k_{\rho\gamma}\frac{1}{p}\right)\Delta\gamma + \mu_\gamma^* \cdot \dot{\gamma}; \quad (24)$$

course angle stabilization

$$\varphi_{tr\,fb} = \left[\left(i_\psi + k_{\rho\psi}\frac{1}{p}\right)\Delta\psi + \mu_\psi \cdot \dot{\psi}\right]\cos\upsilon;$$

where i_υ^*, $k_{\rho\upsilon}$, μ_υ^*, i_γ^*, $k_{\rho\gamma}$, μ_γ^*, i_ψ, $k_{\rho\psi}$ and μ_ψ are the gear ratios.

This technique ensures a possibility to specify manually the velocities of reversal only for the basic control at the flight regime under consideration. However, it takes no account of such peculiarities inherent to a pilot as time necessary for reading information, delay in the controls displacement and other factors.

Modelling non-steady flight regimes

Analysis of data obtained at the flight regime with vertical overloads

A portion of flight data of 80 second in length was analysed. During this interval of time the helicopter twice reached the regime of vertical overloads (zoom). The first peak is at the 623rd second of flight, where $n_y \approx 1.6$.

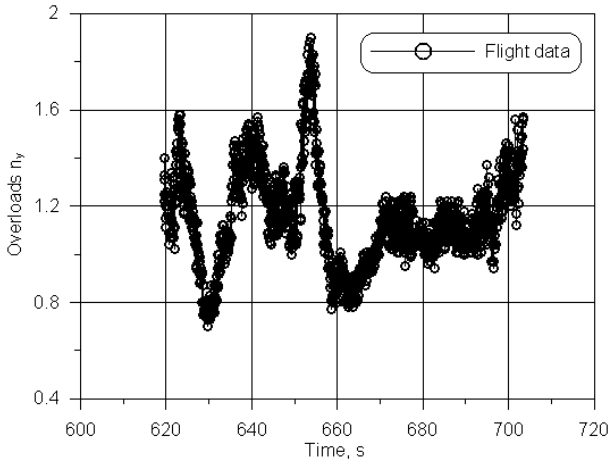

Fig. 2. Flight data on overloads.

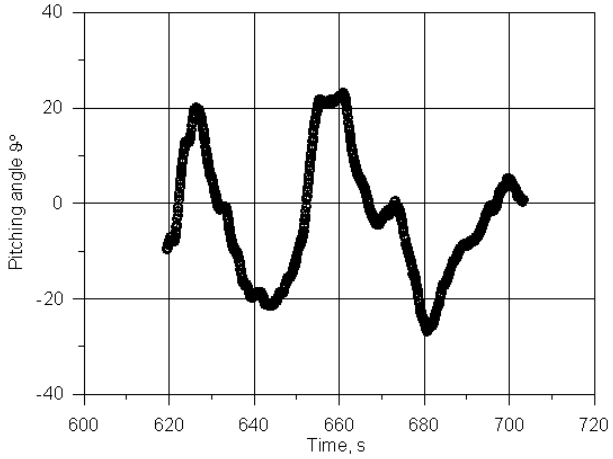

Fig. 3. Flight data on the pitching angle at the vertical overload.

The second peak is at the 655th second of flight, were $n_y \approx 1.9$ (Fig. 2). In this case, the pitching angle varied each time in the range from -20° to

+20° and in descent from the second zoom the pitching angle was -30° (Fig. 3). During this manoeuvre the inclination of a wobble plate ring changed each half-second (Fig. 4).

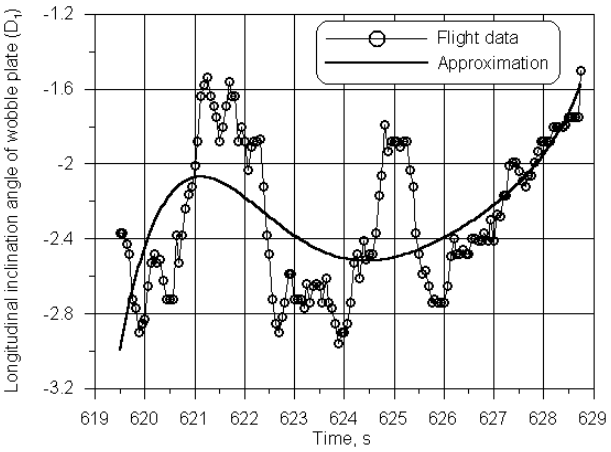

Fig. 4. Longitudinal inclination angle of the wobble plate ring at the vertical overload regime.

Design modelling of the flight regime with vertical overloads and comparison with flight data

Design modelling of the first peak of vertical overloads in the time range from 619 to 629 seconds was carrier out. The basic parameter for flight modelling was a pitching angle. The flight data on the pitching angle at this section start from –10°, then a pilot performs step climb and the pitching angle values at the zoom peak amount to 20° (Fig. 5).In mathematical modelling this manoeuvres is divided into three sections:

1. going into dive;
2. diving turn with zoom;
3. zoom flight.

In calculating these non-steady flight regimes the mathematical model of helicopter motion had four degrees of freedom: horizontal and vertical motion; pitching angular motion, rolling angular motion.

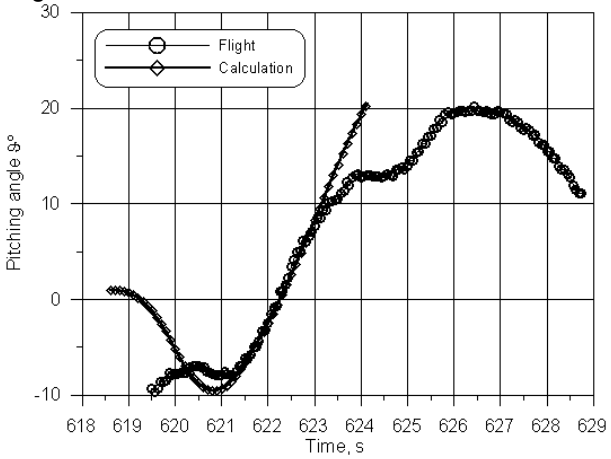

Fig. 5. Helicopter pitching angle.

The mathematical modelling was carried out with the same dynamics of pitch variation as in a real flight (Fig. 5). In this case a good coincidence of overload values (Fig. 6) and bending moments in the thrust plane (Fig. 7 and 8) was obtained – the amplitude of flight data variation is close to design data.

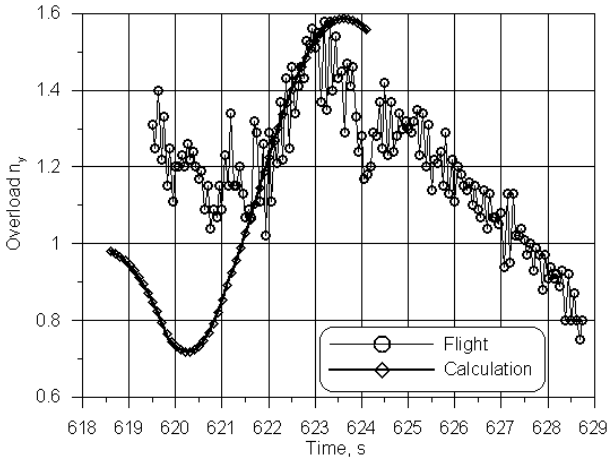

Fig. 6. Vertical overloads.

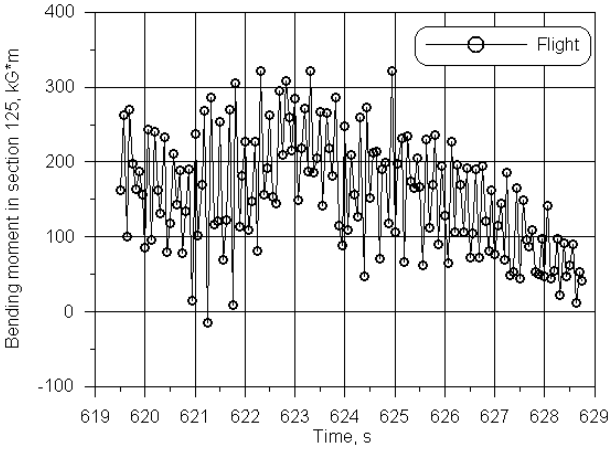

Fig. 7. Bending moment in the flapping plane at 125 mm point from the rotation axis.

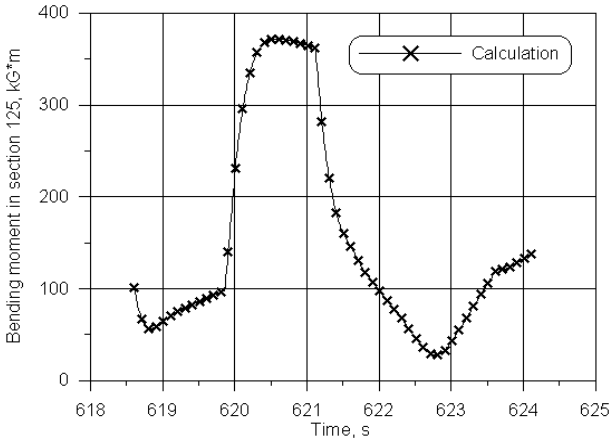

Fig. 8. Design value of bending moments in the flapping plane

Design modelling of the helicopter descent regime

The test modelling of the helicopter descent regime (Fig. 9 and 10) was carried out. Initial position is trim at V_x = 150 km/h. The disturbing factor: the blade pitch φ_{07} decreases by -2; -4; -6; -8 degrees, the pitching angle remains constant.

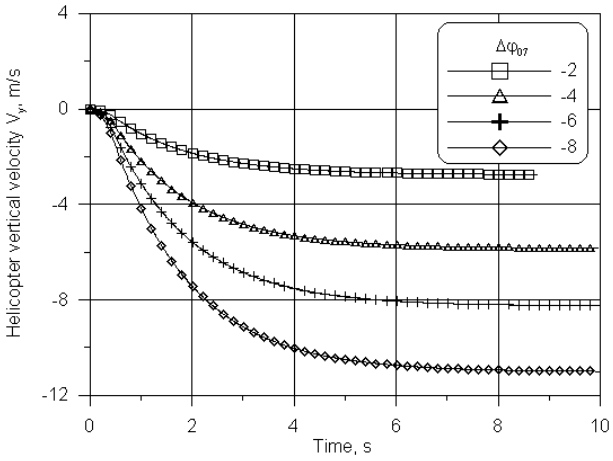

Fig. 9. Helicopter vertical descent velocity

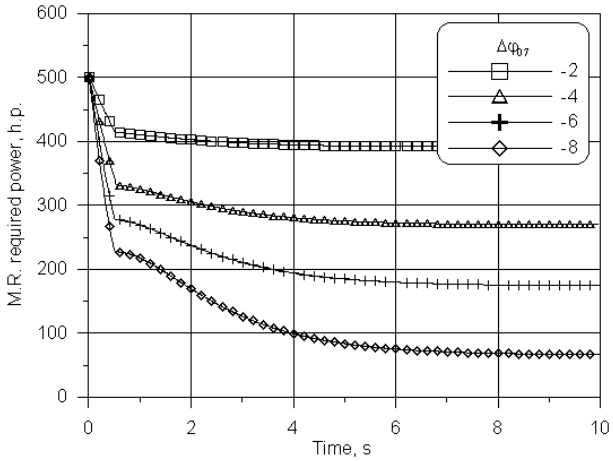

Fig. 10. Main rotor required power at the helicopter descent regime

The flight calculation for the helicopter descent regime at a sharp variation of the pitching angle (Fig. 11) was carried out to study a qualitative effect of the pitching angle on the helicopter descent velocity.

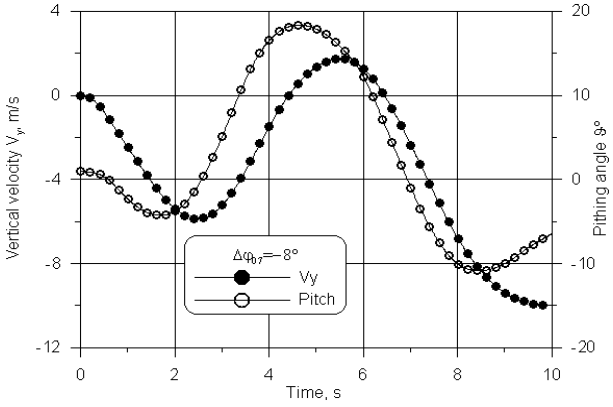

Fig. 11. Helicopter vertical descent velocity as a function of the pitching angle variation

Design modelling of the helicopter climbing regime

The test modelling of the climbing regime was carried out (Fig. 12 and 13). Initial position is trim at V_x = 150 km/h. The disturbing factor: the blade pitch φ_{07} increases by 2; 4; 6; 8 degrees for 0.5 second.

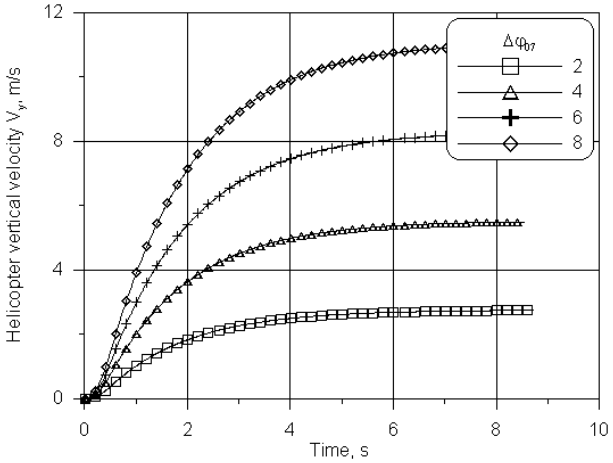

Fig. 12. Vertical climbing velocity

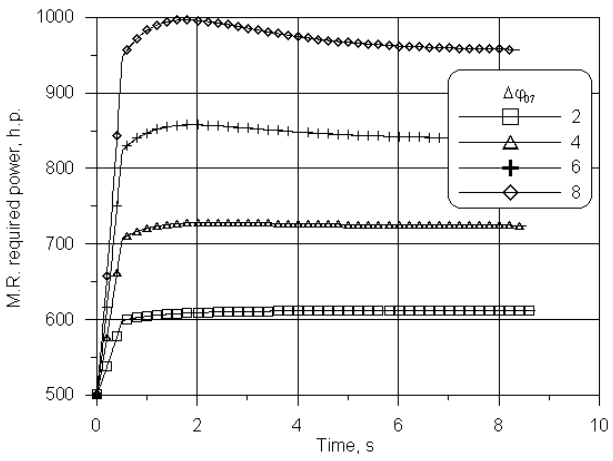

Fig. 13. Main rotor required power at the helicopter climbing regime

Design modelling of the helicopter acceleration regime

The test modelling of the helicopter acceleration regime (Fig. 14 and 15) was carried out.

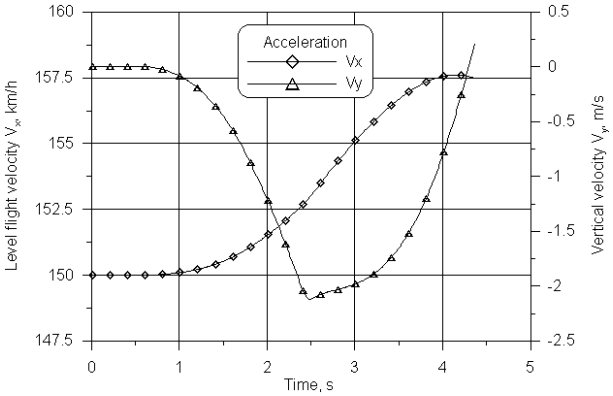

Fig. 14. Helicopter acceleration

The initial position is trim at V_x = 150 km/h. The disturbing factor: the blade pitch φ_{07} increases by 1 degree for 0.5 second the pitching angle remains constant.

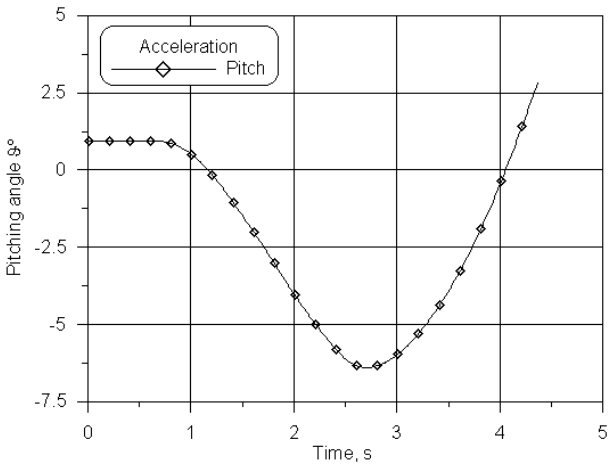

Fig. 15. Helicopter acceleration

Remote control system

The digital redundant electrohydraulic integrated system of the "Ansat" helicopter control provides:

- characteristics of helicopter stability and controllability required by FAR-29;
- manual control of the helicopter angular position in pitch and roll at $V_{in} < 70$ km/h and of the pitching angle at $V_{in} \geq 70$ km/h in the range from $\pm 1^0$ from its steady values;
- manual control of the angular velocities ω_x and ω_z at $V_{in} \geq 70$ km/h and of the angular velocity ω_y over the whole range of flight velocities;
- realization of an advance angle during control over the whole range of flight velocities;
- automatic stabilization of pitching, rolling and course angels over the whole range of flight velocities and altitudes;
- automatic stabilization of the flight indicated velocities at $V_{in} > 70$km/h;
- automatic stabilization of the flight pressure altitude;
- automatic stabilization of the flight geometric altitude;
- automatic coordination of course turn at $V_{in} > 70$km/h in manual and automatic control;
- automatic variation of control kinematics by the common pitch of the tail rotor depending on ambient pressure and temperature;
- automatic change to the analog redundant control at the third failure in the control channel for any steering gear;
- continuous check of normal operation in each of four control channels with the automatic switch of rejected redundancy and data output on this failure.

Mathematical model of a system "helicopter-integrated control system."

The helicopter mathematical model is a linearized mathematical model described above. Linearization is caused by the fact that a great number of calculations must be carried out for minimal possible time to adjust a control system. Such a simplification of the helicopter model may be justified taking also into account that a short-period motion of a helicopter is considered.

The mathematical model of the control system represents the control laws acting in accordance with the system operation logic; it is also a model of the flight control actuator. The model of flight control actuator includes an algorithm for recalculating the specified inclination angles of the wobble plate to actuator rod strokes and an actuator mathematical model that contains models of its electric and hydraulic systems. The values of actuator rod outputs obtained are transformed into real inclination angles of the wobble plate which are transferred to the helicopter mathematical model. The parameters that are autopilot control signals: angles, angular velocities, altitude and others – are taken without regard for measurement errors and their possible filtration.

Objectives and problems of modelling

The basic objectives to be pursued by modelling the control system operation are the following:

- to evaluate the efficiency of control laws;
- to determine the quality of helicopter control provided by the control laws proposed;
- to form suggestions for correction of the structure, operation logic and control laws of the integrated control systems.

Modelling altitude stabilization

The altitude stabilization under the disturbance $\Delta V_y = 2$ m/s at the flight velocity of 250 km/h is shown in Fig. 16. The stabilization law provides the required stabilization since it involves a position error signal of the current and specified altitudes, corrections with respect to the altitude variation speed and its error integral, as well as to the pitching angle and its angular velocity.

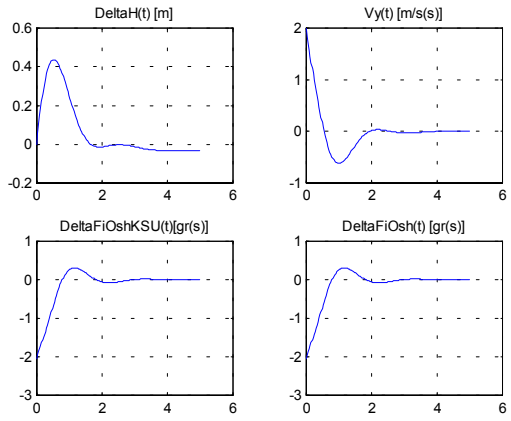

Fig. 16 Altitude stabilization at V = 250 km/h

Stabilization of the helicopter angular motion

In modelling the stabilization regimes for the angles ϑ, γ and ψ disturbance was specified in each individual channel. In this case motion was stabilized in all three channels.

The helicopter angular motion stabilization was modelled under disturbances $\Delta V_y = 10$ m/s

and $\Delta V_z = 10$ m/s. The results of modelling at hovering V = 0 km/h and at the velocity V = 250 km/h when the disturbance $\Delta V_y = 10$ m/s is specified are shown if Fig. 17 and 18.

It is seen that the stabilization quality meets all requirements within the entire range of velocities considered. The transient process is of an aperiodic character with a high speed of response.

The helicopter stabilization at hovering under the disturbance $\Delta\vartheta = 3$ degrees is shown in Fig. 19. It is seen that this disturbance is properly controlled.

The following note is advisable. When choosing the gear ratios the controls travels due to the automatic control circuits must be as small as possible. The point is that the control laws and gear ratios at the beginning of their adjustment during flight tests are assigned on the assumption that the models of an object and controller properly correspond to a full-scale vehicle. Actually, it may be contrary to fact and at a certain degree of inconsistency between a model and a full-scale vehicle may result in emergency conditions due to the unstable inconsistent process. For this purpose, the input signals of automatic equipment must be limited during flight test.

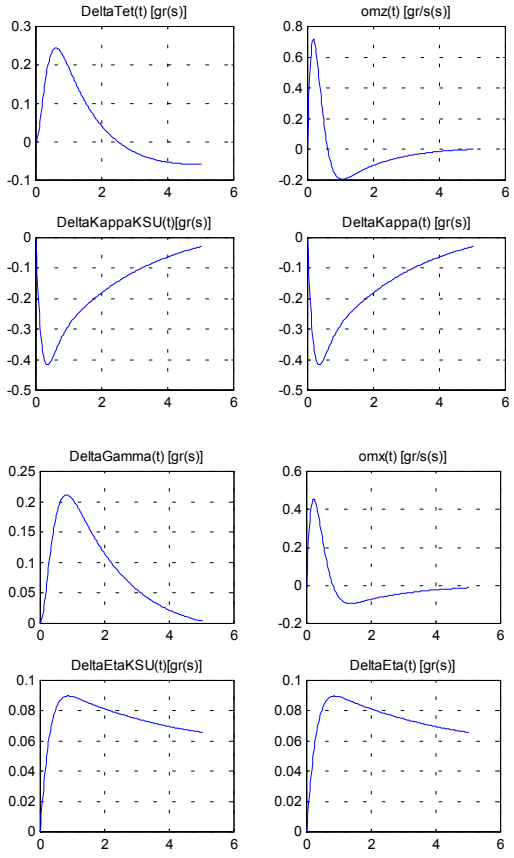

Fig. 17 Angular motion stabilization. Disturbance $\Delta V_y = 10$m/s. Hovering.

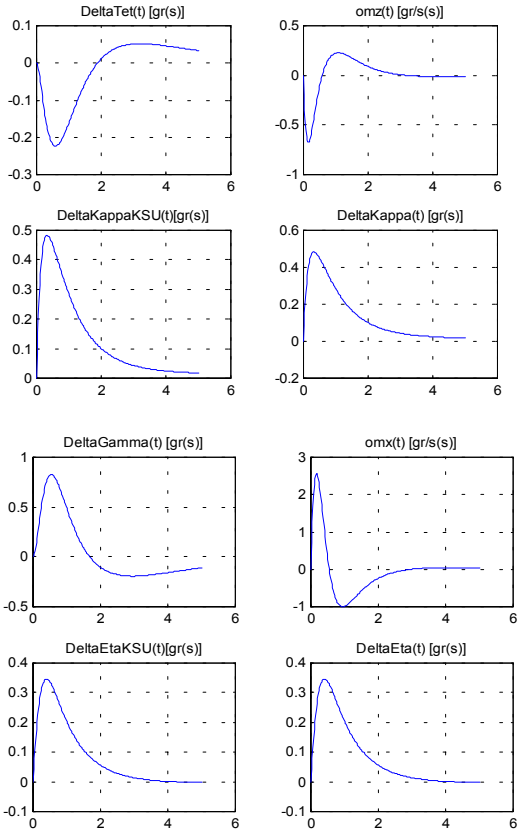

Fig. 18 Angular motion stabilization. Disturbance $\Delta V_y = 10$m/s. V = 250 km/h.

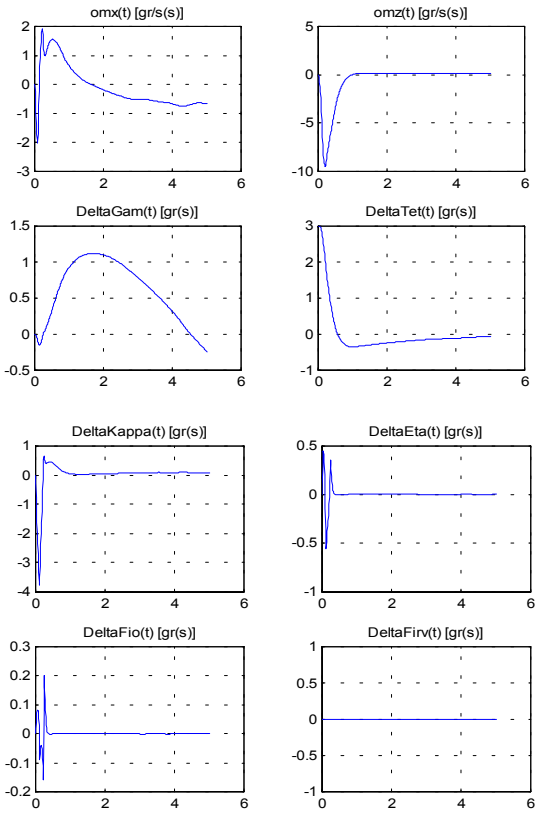

Fig. 19 Pitching angle stabilization. Disturbance. $\Delta\vartheta = 3$ degree. Hovering.

Velocity stabilization

The stabilization law for the current indicated velocity is a law for stabilizing the specified pitching angle that is formed as an error signal of the current and specified velocities as well as this error integral. In the velocity stabilization circuit provision is made for limitation of the signal $\Delta\vartheta$. The calculations show that this limitation must not exceed 2° or 3°. The velocity stabilization under the disturbance ΔV_x = 10 m/s is shown in Fig. 20. The angles γ and ψ were stabilized concurrent with the velocity. The transient process was considered over a limited time interval but the proper character of the velocity stabilization law proposed is beyond question.

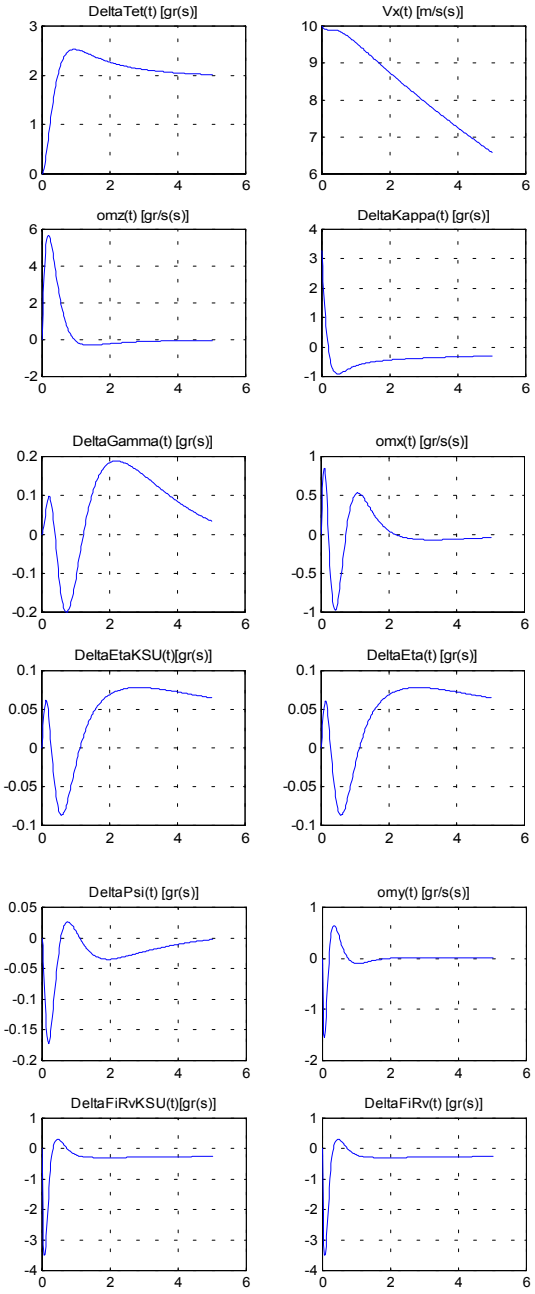

Fig. 20 Velocity stabilization. Disturbance ΔV_x = 10m/s. V = 250km/h

Automatic turn

Figures 21 and 22 present the results of modelling a regime of coordinated automatic turn for flight velocities V = 100 km/h and V = 250 km/h. The specified angle of turn is ψ_{sp} = 20°.

It is seen that for the flight velocities indicated the automatic turn is made with a small deviation of the pitching angle, flight altitude and velocity from the corresponding initial values. During turn the rolling angle varies according to the yaw angle error. In this case, the maximum value of lateral overload (at the beginning entry into a manoeuvres) increases as the flight velocity grows.

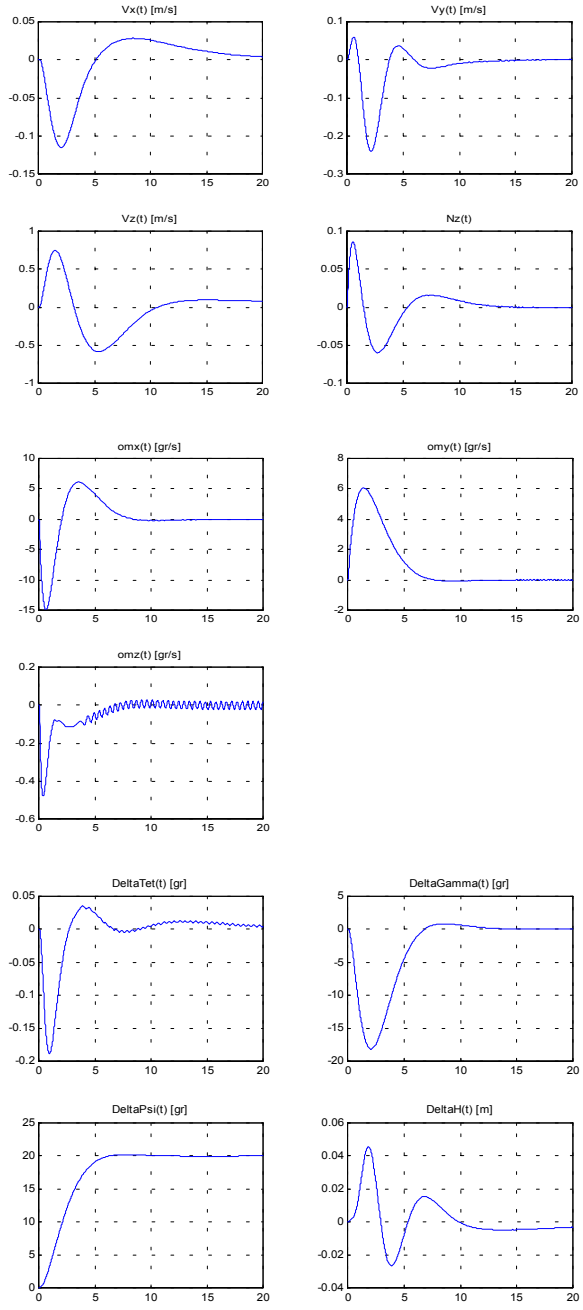

Fig. 21 Automatic turn, ψ_{sp} = 20°, V = 100 km/h.

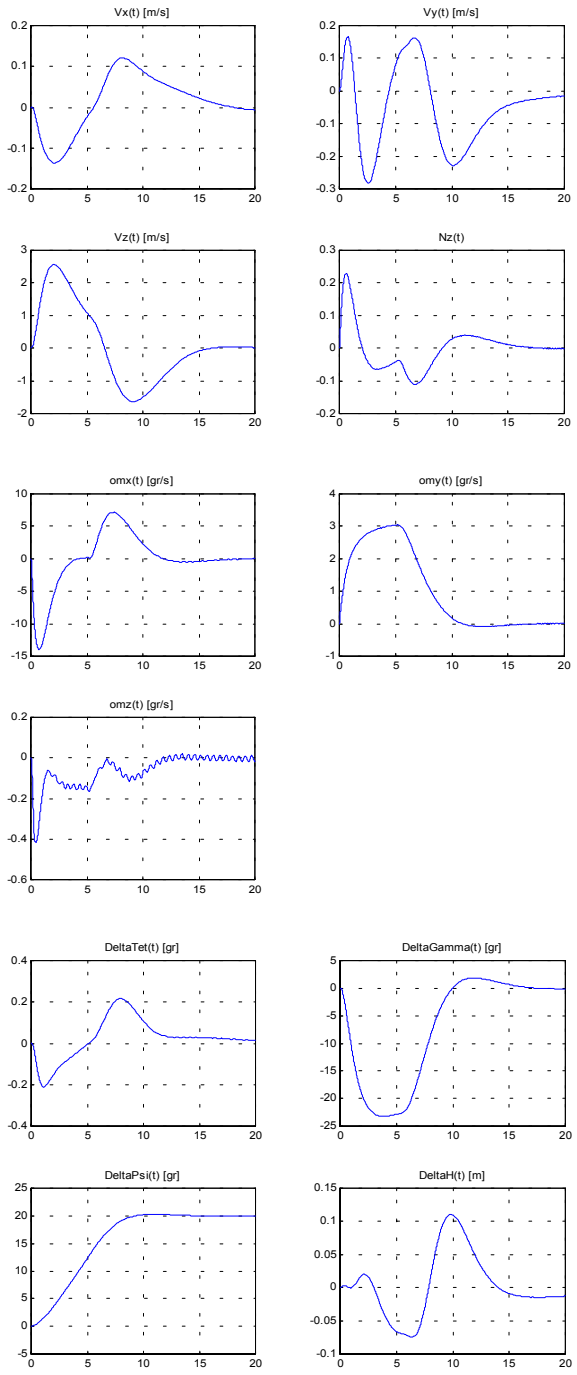

Fig. 22 Automatic turn, ψ_{sp} = 20°, V = 200 km/h

Manual coordinated turn

In modelling the manual coordinated turn the pilot's operation along the roll channel was simulated by specifying the definite values of the rolling angle in the stabilization circuit for this angle. The results of modelling the regime of manual coordinated turn during the time specified (Δt = 20 s) for flight velocities V = 100 km/h and V = 250 km/h are given in Fig. 23 and 24.

It is seen that for the flight velocities selected the manual turn is made with a small deviation of the pitching angle, flight altitude and velocity from the corresponding initial values. As at the regime of automatic turn, the maximum value of the overload N_z at entry into the manoeuvre with velocity V = 100 km/h is essentially smaller that its maximum value for V = 250 km/h. For the angle $\Delta\gamma_{sp}$=20° these values are $N_z \cong$ -0.07 and $N_z \cong$ -0.2, respectively.

At the same time, after the rolling angle reaches the specified value, the manoeuvre is executed with zero value of lateral overload and a constant value of the angular velocity ω_y; along with the insignificant deviation of the pitching angle, flight altitude and velocity from the corresponding initial values this fact indicates that the turn is made with reasonable quality of coordination.

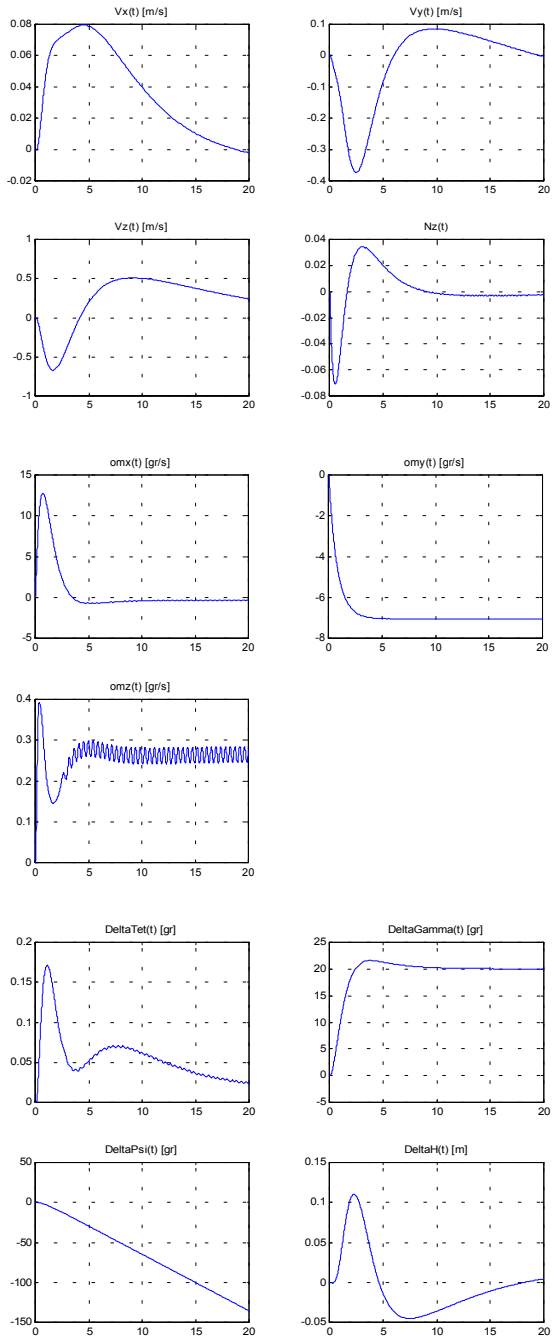

Fig. 23 Manual turn, γ_{sp} = 20°, V = 100 km/h

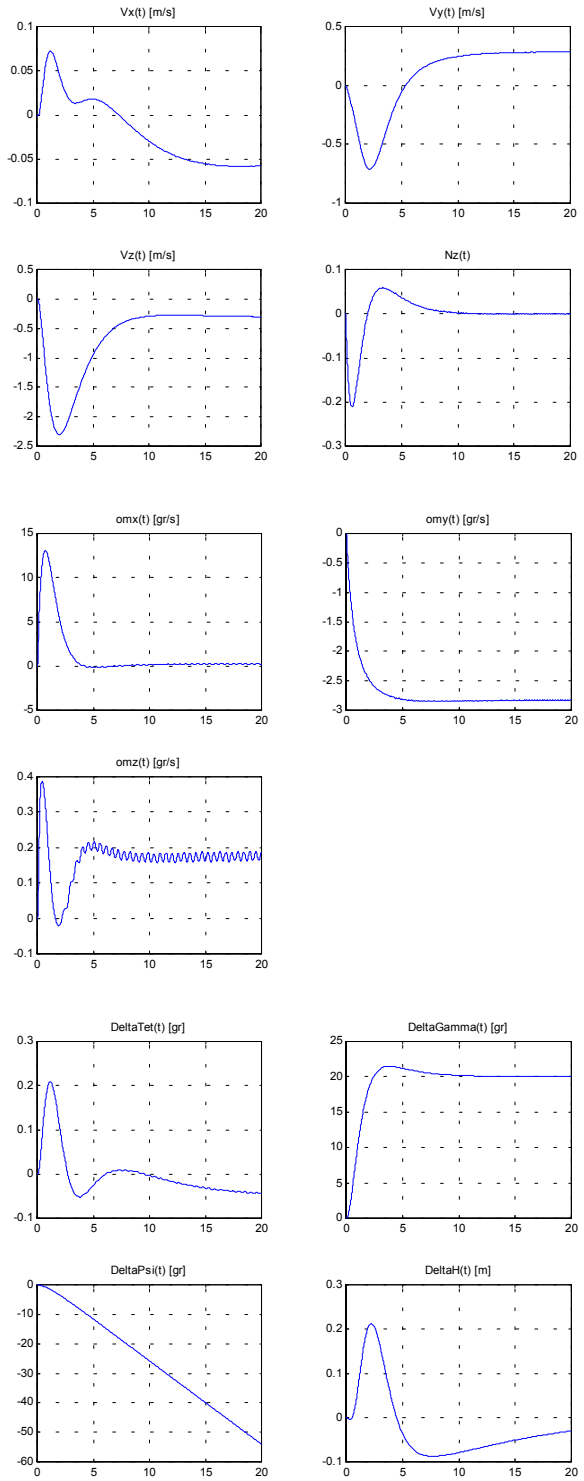

Fig. 24 Manual turn, γ_{sp} = 20°, V = 250 km/h

References

1 A.M.Girfanov, S.A.Mikhailov, and E.I.Nikolaev, “Study of the effect hingeless main rotor elastic blades on torsion loading”, Proceedings of the Russian Helicopter Society IV-th Forum, Moscow, 2000.

2 W. Johnson, Helicopter Theory, in two book, [Russian translation] Vol. 1, Mir, Moscow, 1983.

3. A.S.Braverman and A.P. Waintraub, Helicopter Dynamics. Limiting Flight Regimes, Mashinostroenie, Moscow, 1988.

4. V.A. Kozhevnikov, Automatic Stabilization of Helicopters, Mashinostroenie, Moscow, 1978.

5. A.P.S. Bramvel, Helicopter dynamics, [Russian translation], Mashinostroenie, Moscow, 1982

6. A.M.Girfanov, Aeroelastic calculation and balancing of a single-rotor helicopter with a hingeless main rotor, Candidate of technical sciences dissertation, Kazan, 2000.